

pubs.acs.org/cm Article

Kinetic Trapping of Photoluminescent Frameworks During High-Concentration Synthesis of Nonemissive Metal—Organic Frameworks

Arjun Halder, David C. Bain, Tristan A. Pitt, Zixiao Shi, Julia Oktawiec, Jung-Hoon Lee, Stavrini Tsangari, Marcus Ng, José J. Fuentes-Rivera, Alexander C. Forse, Tomče Runčevski, David A. Muller, Andrew J. Musser, and Phillip J. Milner*



Cite This: Chem. Mater. 2023, 35, 10086-10098



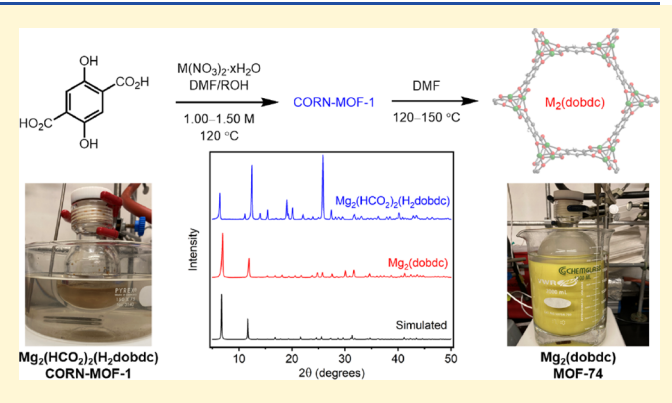
ACCESS

III Metrics & More

Article Recommendations

Supporting Information

ABSTRACT: Metal—organic frameworks (MOFs) are porous, crystalline materials constructed from organic linkers and inorganic nodes with potential utility in gas separation, drug delivery, sensing, and catalysis. Small variations in the MOF synthesis conditions can lead to a range of accessible frameworks with divergent chemical or photophysical properties. New methods to controllably access phases with tailored properties would broaden the scope of MOFs that can be reliably prepared for specific applications. Herein, we demonstrate that simply increasing the reaction concentration during the solvothermal synthesis of $M_2(dobdc)$ ($M=Mg,Mn,Ni;\ dobdc^4=2,5\text{-dioxido-1,4-benzenedicarboxylate}$) MOFs unexpectedly leads to trapping of a new framework termed CORN-MOF-1 (CORN = Cornell



University) instead. In-depth spectroscopic, crystallographic, and computational studies support that CORN-MOF-1 has a structure similar to that of M_2 (dobdc) but with partially protonated linkers and charge-balancing or coordinated formate groups in the pores. The resultant variation in linker spacing causes CORN-MOF-1 (Mg) to be strongly photoluminescent in the solid state, whereas H_4 dobdc and Mg_2 (dobdc) are weakly emissive due to excimer formation. In-depth photophysical studies suggest that CORN-MOF-1 (Mg) is the first MOF based on the H_2 dobdc²⁻ linker that likely does not emit via an excited-state intramolecular proton transfer (ESIPT) pathway. In addition, CORN-MOF-1 variants can be converted to high-quality samples of the thermodynamic M_2 (dobdc) phases by heating in N_1N -dimethylformamide (DMF). Overall, our findings support that high-concentration synthesis provides a straightforward method to identify new MOFs with properties distinct from known materials and to produce highly porous samples of MOFs, paving the way for the discovery and gram-scale synthesis of framework materials.

INTRODUCTION

Selectively isolating a single phase with tailored properties from a reaction mixture in which multiple phases can form is a fundamental challenge in materials synthesis. This challenge is illustrated by metal-organic frameworks (MOFs), which are porous crystalline materials constructed from polytopic organic linkers and inorganic nodes with potential utility for chemical separations, catalysis, drug delivery, sensing, and beyond. 1-4 Because metals can form multiple nodes and linkers can access distinct protonation states or coordination modes, many frameworks can potentially form from the combination of a given metal salt and linker. 5-8 As such, small variations in the synthesis conditions can lead to drastically different reaction outcomes. Controlling the topology of a framework is critical, as small changes in the framework architecture can have a profound influence on physical properties. Due to these limitations, MOF syntheses are often optimized on a trial-anderror basis, contributing to the perception that their synthesis remains a "black box". $^{8-10}$

To ensure phase purity, MOFs are typically prepared under thermodynamic control, which involves synthesis under dilute solvothermal conditions at high reaction temperatures to maximize the reversibility of framework self-assembly. Unfortunately, the large solvent volumes required for traditional solvothermal synthesis necessitate the use of liters of solvent to produce grams of MOF, contributing greatly to the cost of MOFs on scale and generating significant waste. ¹¹

Received: August 20, 2023 Revised: October 27, 2023 Accepted: October 27, 2023 Published: November 20, 2023





High-concentration solvothermal synthesis would enable MOF production with reduced solvent use, but mixtures of phases¹² or low-quality materials^{13–16} are generally obtained under these conditions; successful syntheses of porous, phase-pure MOFs under high-concentration conditions (>0.25 M in linker) without seeding remain remarkably rare.^{17–20} Concentration-dependent selection between distinct MOF phases has also not been reported to date.

The MOF-74, CPO-27, or M_2 (dobdc) (M = Mg, Mn, Fe, Co, Ni, Cu, Zn, Cd; dobdc⁴⁻ = 2,5-dioxido-1,4-benzenedicarboxylate) family of frameworks embodies the aforementioned synthetic challenges (Figure 1). These materials

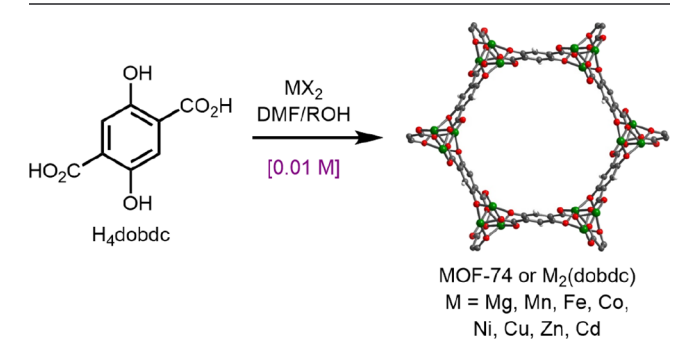


Figure 1. Standard synthesis of M_2 (dobdc) under dilute solvothermal conditions (concentration of the linker shown). R = alkyl, H.

represent a canonical family of frameworks due to their promise for chemical separations, 25,26 gas storage, 23 and catalysis, 27,28 yet they are typically prepared under dilute solvothermal conditions (\sim 0.01 M). In addition, variations in solvent, temperature, metal precursor, and other synthesis parameters have been shown to produce a range of different Mg, $^{29-35}$ Mn, 36,37 Ni, 38 Co, $^{38-41}$ Cu, 25 and Zn $^{41-47}$ phases. Notably, some of these frameworks exhibit detectable photoluminescence (PL) in the solid state, $^{29-31,35,36,48}$ demonstrating that small changes in the linker protonation state or spatial orientation can have a profound effect on framework photophysical properties. A critical barrier to predicting the preferred phase(s) is a lack of chemical insight into the processes underpinning M_2 (dobdc) self-assembly. $^{9,49-51}$ For example, while stepwise linker deprotonation (H_4 dobdc $\rightarrow H_2$ dobdc $^{2-}$ \rightarrow dobdc $^{4-}$) through distinct phases has been established under mechanochemical conditions with basic metal precursors, 44,52 its general role in M_2 (dobdc) formation under solvothermal conditions remains unclear.

Herein, we demonstrate that increasing the linker concentration in $M_2(dobdc)$ (M=Mg,Mn,Ni) syntheses induces the clean formation of a new microporous phase, $M_2(HCO_2)_2(H_2dobdc)$ or CORN-MOF-1 (CORN = Cornell University), with partially protonated linkers. To the best of our knowledge, this represents the first example of a phase-to-phase transition induced by changing *only* the concentration of a MOF synthesis. Moreover, CORN-MOF-1 (Mg) is intensely

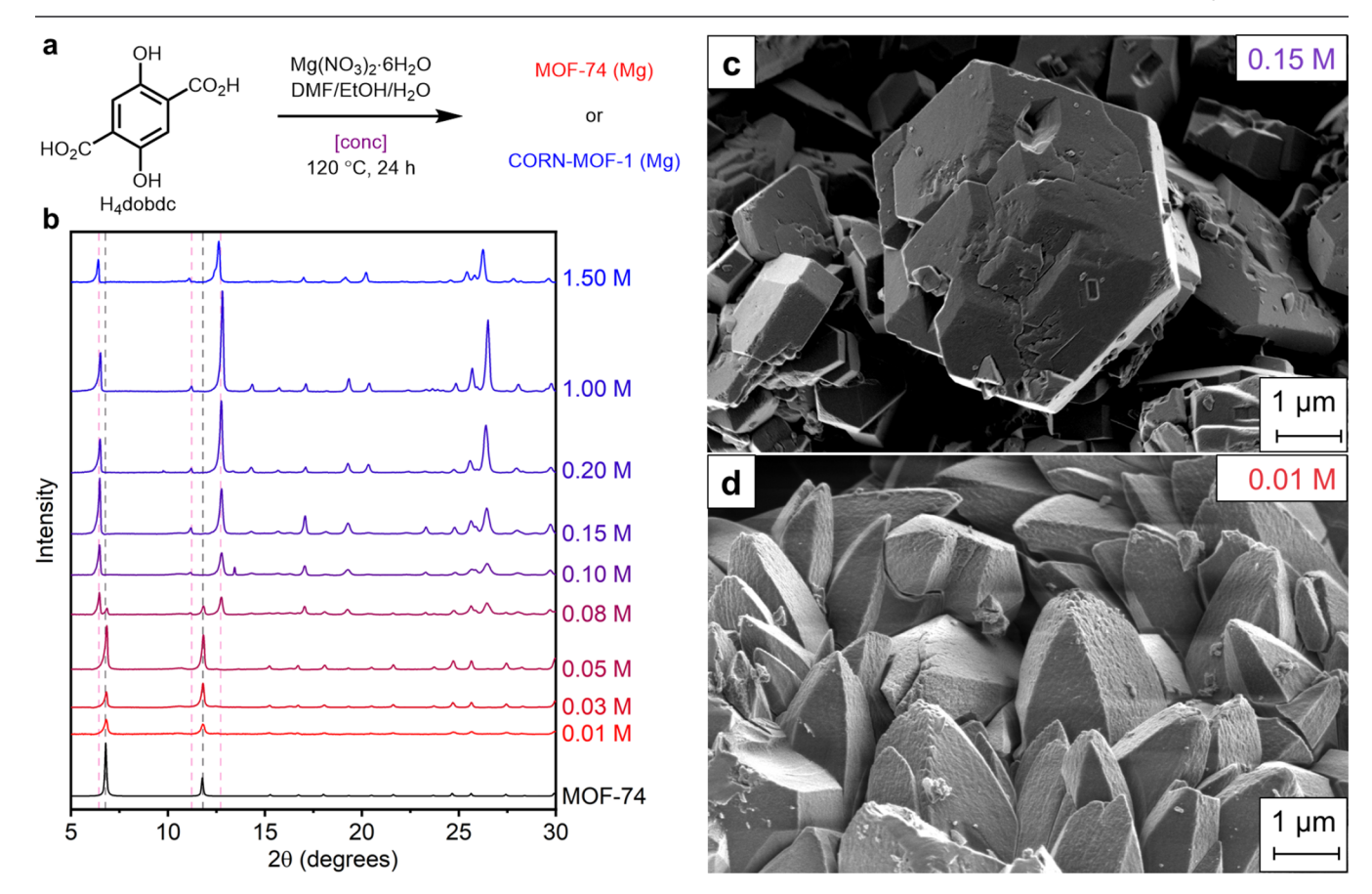


Figure 2. (a) Synthesis of $Mg_2(dobdc)$ and/or CORN-MOF-1 (Mg) at varying linker concentrations. (b) PXRD patterns at increasing reaction concentrations. Transition from $Mg_2(dobdc)$ (dashed gray lines) to CORN-MOF-1 (Mg) (pink circles) is indicated. The pattern corresponding to the previously reported SCXRD structure of $Zn_2(dobdc)$ is included for reference (black). (c) SEM image of CORN-MOF-1 (Mg) synthesized at 0.15 M with stirring. (d) SEM image of $Mg_2(dobdc)$ synthesized at 0.01 M without stirring.

photoluminescent in the solid state while H_4 dobdc and Mg_2 (dobdc) are nearly nonemissive. In-depth photophysical studies suggest that this is due to nonradiative excimer formation in H_4 dobdc and Mg_2 (dobdc) that is absent in CORN-MOF-1 (Mg). As such, our work demonstrates that high-concentration solvothermal synthesis provides a straightforward avenue to reduce the amount of solvent required to prepare MOFs, isolate new phases that provide mechanistic insight into MOF formation, and discover new materials with distinct (photo)physical properties compared with known thermodynamic phases.

■ RESULTS AND DISCUSSION

Owing to its high density of coordinatively unsaturated Mg²⁺ sites and low molecular weight, Mg₂(dobdc) exhibits high adsorption capacities for many gases.^{22,25,53} As such, it is a promising material for applications in chemical separations and gas storage.^{26,54,55} Decreasing the volume of solvent required to prepare high-quality Mg₂(dobdc) would facilitate its gram-

High-Concentration Synthesis of CORN-MOF-1 (Mg).

gas storage. 26,54,55 Decreasing the volume of solvent required to prepare high-quality $Mg_2(dobdc)$ would facilitate its gramscalable synthesis, especially by nonspecialists. However, previous reports suggest that even a slight increase in the $Mg_2(dobdc)$ synthesis concentration (up to 0.05 M in linker) without stirring leads to a mixture of nonporous phases. Therefore, we asked the following question: can $Mg_2(dobdc)$

actually be synthesized at high reaction concentrations? Solvothermal syntheses of $Mg_2(dobdc)$ in an 18:1:1 mixture

of N_1N_2 -dimethylformamide (DMF), ethanol (EtOH), and H_2O at 120 °C for 24 h^{22} were carried out at linker concentrations ranging from 0.01 to 1.50 M with 2.50 equiv of $Mg(NO_3)_2 \cdot 6H_2O$ at every concentration (Figure 2a,b, Supporting Information or SI Figure S1, see SI Section 3 for details). Notably, vigorous stirring (700 rpm) was required to

produce samples free from inorganic impurities, such as

 $Mg(HCO_2)_2$.

At H₄dobdc concentrations between 0.01 and 0.05 M, phase-pure Mg₂(dobdc) was obtained, as confirmed by comparison of the PXRD pattern to that simulated from the single-crystal X-ray diffraction (SCXRD) structure of Zn₂(dobdc).⁵⁶ Intriguingly, simply increasing the linker concentration to 0.08 M led to contamination of Mg₂(dobdc) with a new phase, which we term as CORN-MOF-1 (Mg). We hypothesize that CORN-MOF-1 (Mg) is a kinetic phase closely related in structure to $Mg_2(dobdc)$. Indeed, higher reaction temperatures (140-160 °C) were found to favor Mg₂(dobdc) over CORN-MOF-1 (Mg) at an intermediate linker concentration of 0.08 M (SI entry Figure S31). The PXRD pattern of this material does not match any known crystalline phase constructed from Mg²⁺ ions and H₂dobdc²⁻ or dobdc⁴⁻ linkers (SI Figure S2). At reaction concentrations between 0.10 and 1.50 M, only phase-pure CORN-MOF-1 (Mg) is obtained. The transition from Mg₂(dobdc) to CORN-MOF-1 (Mg) was also evident by scanning electron microscopy (SEM) (Figure 2c,d). Hexagonal needles/rods characteristic of M₂(dobdc) materials²⁴ were obtained at low concentrations (Figure 2d), whereas hexagonal plates corresponding to CORN-MOF-1 (Mg), along with other less welldefined crystallites, were obtained at higher reaction concentrations (Figure 2c, SI Figure S13). This synthesis could be reproducibly carried out on a 15 mmol scale using only 10 mL of organic solvent to yield >5 g of CORN-MOF-1 (Mg) in a single batch (SI Figure S3). Notably, the same phase change was observed in 1:1 DMF:methanol (MeOH), another

solvent system commonly used to prepare $Mg_2(dobdc)$ analogues, ⁵⁷ as confirmed by PXRD and SEM (SI Section 6). These results indicate that a clean phase change from $Mg_2(dobdc)$ to CORN-MOF-1 (Mg) is generally favored at high reaction concentrations.

Due to the unusual conditions under which CORN-MOF-1 (Mg) forms—high reaction concentrations with vigorous stirring—we have been unable to grow sufficiently large crystals of this material to enable structural elucidation by SCXRD. Attempts to determine the structure of CORN-MOF-1 (Mg) via electron diffraction were only partially successful (SI Section 16). The collected reflections match well to those observed by PXRD, but only a partial data set could be collected due to the anisotropic nature of the platelike crystals of CORN-MOF-1 (Mg) (Figure 2c). Therefore, the structure of this MOF was interrogated using PXRD (Figure 3) and a host of spectroscopic and analytical methods (Figure 4).

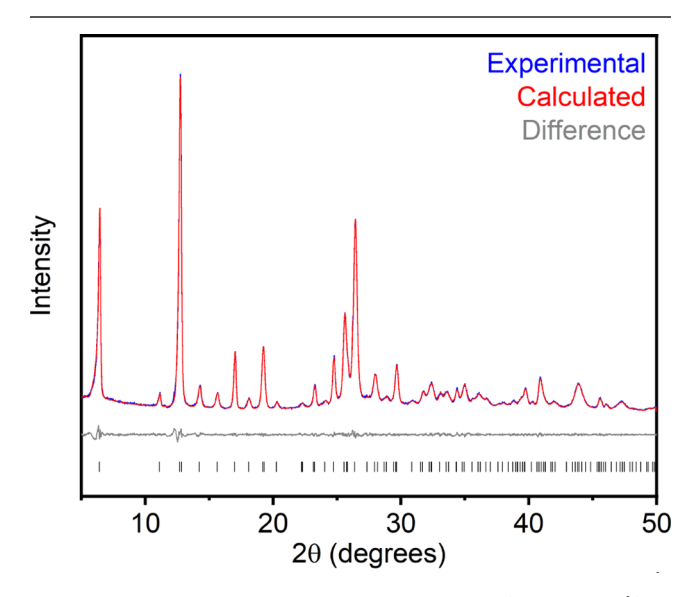


Figure 3. Pawley refinement of the PXRD pattern ($\lambda = 1.5406$ Å) of CORN-MOF-1 (Mg). The shown fit corresponds to the $R\overline{3}$ space group with a = 27.612(2) and c = 7.2853(3) Å. $R_{\rm wp} = 3.85\%$. The black dots indicate calculated Bragg peak positions.

Pawley refinement of the PXRD pattern of CORN-MOF-1 (Mg) prepared at a reaction concentration of 0.1 M revealed that it could be fit well ($R_{\rm wp}=3.85\%$) as a single phase in the $R\overline{3}$ space group (the same space group as Mg₂(dobdc)) with a=27.612(2) Å and c=7.2853(3) Å (Figure 3, SI Section 18). We note that the R3, $R\overline{3}$, R32, R3m, and $R\overline{3}m$ space groups cannot be differentiated using PXRD alone. These unit cell parameters are similar to those previously reported for Mg₂(dobdc) ($R\overline{3}$, a=25.865(4) Å, c=6.911(1) Å)⁵⁸ but slightly expanded in a and c, which accounts for the lower-angle first reflection of CORN-MOF-1 (Mg) compared to Mg₂(dobdc) (Figure 2b). Similar parameters were determined for samples prepared at reaction concentrations of 0.2 and 1.5 M (SI Section 18).

We have consistently observed that the lowest angle reflection in the PXRD pattern of well-activated $M_2(dobdc)$ frameworks $(2\theta \approx 6.8^\circ)$, which corresponds to the $(2\bar{1}0)$ plane, is the most intense reflection (see Figure S28 for an example). Accordingly, this plane contains a large portion of the linker molecules. In contrast, the most or second-most intense reflection in the PXRD pattern of CORN-MOF-1

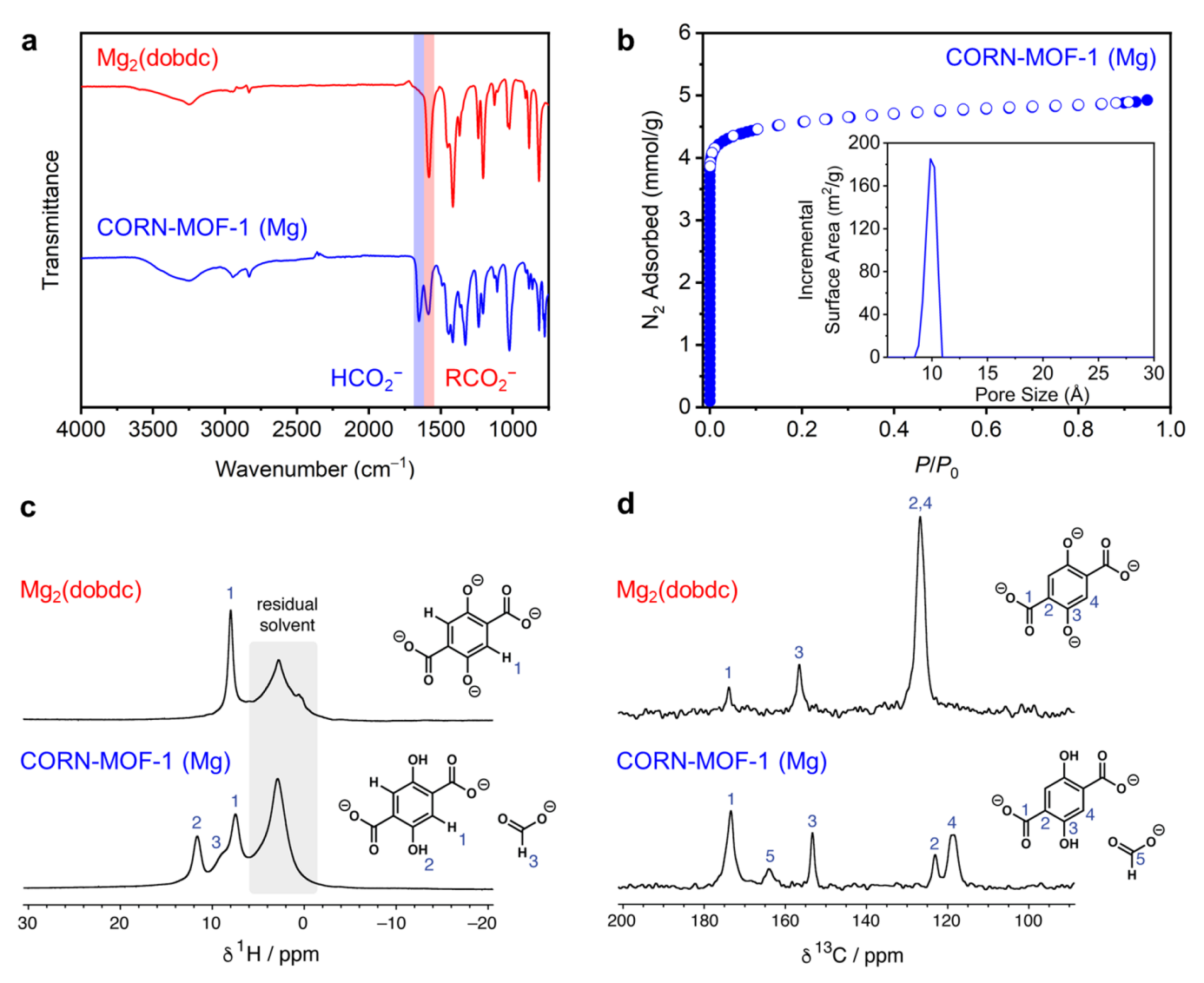


Figure 4. (a) ATR-IR spectra of $Mg_2(dobdc)$ and CORN-MOF-1 (Mg). (b) 77 K N_2 adsorption (closed circles) and desorption (open circles) isotherms of activated CORN-MOF-1 (Mg). Inset: DFT-calculated pore size distribution of CORN-MOF-1 (Mg), assuming a cylindrical pore shape with a metal oxide surface. (c) 1H and (d) CP ^{13}C MAS SSNMR spectra of $Mg_2(dobdc)$ and CORN-MOF-1 (Mg). All SSNMR data were collected at a field strength of 9.4 T and an MAS rate of 25 kHz.

(Mg) is generally observed at $2\theta \approx 12.8^{\circ}$, which corresponds to the (101) plane. The (4 $\overline{2}0$) reflection is found on the right shoulder of this reflection and may contribute to its overall intensity, but its contribution is likely minimal because their combined peak shape is that of a well-defined single reflection originating from the (101) plane. In the $R\overline{3}$ space group, the (101) plane is roughly perpendicular to the c axis and the (2 $\overline{1}0$) plane is parallel to it, meaning that in Mg₂(dobdc), the (101) plane includes the pore volume and the (2 $\overline{1}0$) plane draws a narrow line through it. As such, this qualitative argument indicates that CORN-MOF-1 (Mg) likely contains significant electron density within the framework pores (i.e., more atoms in the (101) plane) that is absent in Mg₂(dobdc). Unfortunately, the disordered nature of this electron density precludes an exact structure solution by PXRD.

In order to gain further insight into the chemical species occupying the pores of CORN-MOF-1 (Mg), this material was characterized by attenuated total reflectance infrared (ATR-IR) spectroscopy after extensive washing to remove residual DMF from the pores (Figure 4a, SI Figure S4 and Table S2).

CORN-MOF-1 (Mg) contains an additional carbonyl C=O stretch (1655 cm^{-1}) that is absent in $Mg_2(dobdc)$. The same C=O stretch (1644 cm⁻¹) was observed by transmission IR after activation of CORN-MOF-1 (Mg) under a vacuum (SI Figure S5), suggesting that it does not correspond to trapped solvent. Based on its frequency,⁵⁹ we hypothesize that this additional carbonyl stretch is due to formate (HCO₂⁻). Indeed, acidic digestion of CORN-MOF-1 (Mg) reproducibly yielded a 1:2 mixture of H₄dobdc and formic acid, as confirmed by solution-state ¹H and ¹³C NMR (SI Figures S6-S8). Residual DMF was not detected nor was a significant amount of HCO2H observed in an acid-digested sample of Mg₂(dobdc) prepared under traditional solvothermal conditions (SI Figure S8). Accounting for charge-balancing and the observed formate:linker ratio, these findings are consistent with a potential (desolvated) molecular formula of Mg₂(HCO₂)₂(H₂dobdc) for CORN-MOF-1 (Mg). Combustion elemental analysis of this material yielded C (32.09%) and H (3.49%) values that are in reasonable agreement with the molecular formula $Mg_2(HCO_2)_2(H_2dobdc)(H_2O)_2$ (32.39%

C, 2.72% H), assuming partial hydration under ambient conditions (SI Table S3). This molecular formula would indicate that the phenols of the linker are protonated in CORN-MOF-1 (Mg), with charge-balancing or coordinated formate groups in the pores. The observed formates likely result from DMF decomposition during MOF formation. Consistently, CORN-MOF-1 (Mg) could be prepared in *N*,*N*-diethylformamide but not in *N*,*N*-dimethylacetamide at any concentration (SI Figures S36 and S37).

The presence of additional species within the pores of CORN-MOF-1 (Mg) is further supported by N2 adsorption measurements at 77 K (Figure 4b). Soaking as-synthesized CORN-MOF-1 (Mg) in MeOH and dichloromethane enabled its desolvation under a high vacuum at 30 °C without significant loss in crystallinity (SI Figure S12). The 77 K N₂ adsorption/desorption isotherms of CORN-MOF-1 (Mg) confirm that it is microporous, with Brunauer-Emmett-Teller (BET) and Langmuir surface areas of 403 and 479 \pm 1 m²/g, respectively (Figure 4b, SI Figures S9 and S10). CORN-MOF-1 (Mg) is the highest surface area Mg-based MOF containing H₂dobdc²⁻ linkers that has been reported to date (SI Table S11). The BET surface area of this material is smaller than that reported for Mg₂(dobdc) (1743 m²/g).⁵⁴ Likewise, the density functional theory (DFT)-calculated pore size distribution of CORN-MOF-1 (Mg) assuming a cylindrical pore shape with a metal oxide surface is ~9.9 Å (Figure 4b inset, SI Figure S11), which is smaller than the crystallographically determined pore aperture of Mg₂(dobdc) (11 Å). Together, these findings support the idea that CORN-MOF-1 (Mg) possesses smaller guest-accessible pores than Mg₂(dobdc), likely due to partial pore-filling by formate groups.

The presence of additional charge-balancing formate groups in CORN-MOF-1 (Mg) was corroborated by magic angle spinning (MAS) ¹H and cross-polarized (CP) ¹³C solid-state NMR (SSNMR) spectroscopies (Figure 4c,d, SI Section 14). As expected, the ¹H and ¹³C MAS SSNMR spectra of Mg₂(dobdc) and CORN-MOF-1 (Mg) possess several resonances that can be assigned to the aromatic linker. Additionally, the ¹H and ¹³C MAS SSNMR spectra of CORN-MOF-1 (Mg) contain resonances at 9 and 164 ppm, respectively, that are absent from the corresponding spectra of Mg₂(dobdc). These resonances can be assigned to the extra formate groups in CORN-MOF-1 (Mg).61 The ¹H MAS SSNMR spectrum of CORN-MOF-1 (Mg) contains another additional resonance at 11.6 ppm, which likely corresponds to phenol groups on the linker. Together with the IR and PXRD data, the SSNMR spectra suggest that CORN-MOF-1 (Mg) is structurally similar to Mg₂(dobdc) but with additional formate groups in the pores along with partially protonated linker molecules.

Further mechanistic studies support the presence of protonated phenols and charge-balancing formate groups in CORN-MOF-1 (Mg) (SI Section 6). The addition of acid (benzoic, acetic, or pivalic acid) to the standard Mg₂(dobdc) synthesis conditions was found to induce the formation of CORN-MOF-1 (Mg) at a relatively low concentration of 0.05 M (SI Figure S38). This is consistent with one of the expected consequences of increasing the reaction concentration, which is to decrease the amount of basic *N,N*-dimethylamine generated *in situ* from DMF decomposition (relative to the linker), and with previous studies suggesting that H₄dobdc is deprotonated stepwise during the self-assembly of

 $M_2(dobdc)$.^{12,44} The addition of acid likely consumes some of the generated N_1N_2 -dimethylamine, favoring partially deprotonated H_2dobdc^{2-} (as in CORN-MOF-1) over fully deprotonated dobdc⁴⁻ (as in MOF-74).

First-principles DFT calculations were carried out to evaluate potential structures for CORN-MOF-1 (Mg) (SI Section 17). A structural model in which each Mg²⁺ center is bound by one bidentate and one bridging formate group (structure A, SI Figure S97) shows the best match to the experimental SSNMR and IR data but a poor match to the experimental PXRD data (SI Figures S99—S101), suggesting that this model accurately reflects the chemical environment of the formates but not their spatial arrangement in the MOF. The mismatch between the experimental and predicted PXRD data may also originate from disordered solvent and/or ligand molecules present in the pores. The disordered pore environment of CORN-MOF-1 (Mg) hinders structural modeling and elucidation by PXRD and remains an active area of investigation in our groups.

Photophysical Analysis of H₄dobdc, CORN-MOF-1 (Mg), and Mg₂(dobdc). The presence of partially protonated linkers in CORN-MOF-1 (Mg) should make this material photoluminescent in the solid state. The H₂dobdc²⁻ linker has been used to prepare a range of photoluminescent MOFs, which are generally proposed to emit via an excited-state intramolecular proton transfer (ESIPT) pathway (Figure S10). 29-31,35,36,48,63-66 Consistently, CORN-MOF-1 (Mg) fluoresces intensely upon irradiation with UV light in the solid state, whereas Mg₂(dobdc) and H₄dobdc emit only weakly (Figure 5a). This initial observation demonstrates how subtle changes in MOF structure—stemming from a simple increase in the synthesis concentration—can significantly modulate MOF photophysical properties. Notably, CORN-MOF-1 (Mg) possesses a BET surface area (403 m²/g) higher than those of all reported photoluminescent MOFs constructed from the H₂dobdc²⁻ linker (Table \$10). In addition, these alternative photoluminescent phases are typically identified by laboriously changing the metal salt, solvent, reaction temperature, and synthesis time (Table S10), whereas CORN-MOF-1 can be obtained by a simple change in the reaction concentration. To understand why CORN-MOF-1 (Mg) fluoresces strongly in the solid state but Mg₂(dobdc) and H₄dobdc do not, detailed PL measurements were carried out (Figures 6 and 7, SI Section 15).

We acquired steady-state PL spectra of H₄dobdc and the two MOFs dissolved or suspended in a range of solvents to evaluate the potential role of the ESIPT pathway (Figure 6ac). As expected, the PL line-shape of H₄dobdc is highly solvent dependent, consistent with the ESIPT mechanism (Figure 6a, see SI Section 15 for further discussion). Crucially, there are no such changes in the UV-vis absorption line-shape across this series, supporting that solvent polarity and hydrogenbonding ability predominantly affect the excited state (i.e., not the ground state) of this molecule (SI Figure S80 and S81). For Mg₂(dobdc) suspended in various solvents, the weak PL is essentially independent of solvent polarity—except for MeOH or H₂O, in which the MOF fully or partially degrades (Figure 6b, SI Figure S79). This result is expected as Mg₂(dobdc) does not have free phenols and thus cannot emit via an ESIPT pathway. Surprisingly, the emission of CORN-MOF-1 (Mg) is similarly solvent-independent (Figure 6c). This suggests that the strong PL either does not occur via ESIPT or that the phenol groups are not accessible to solvent molecules,

a



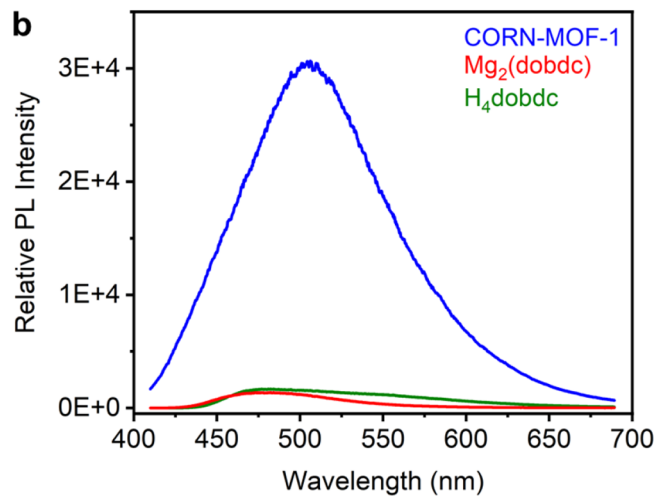


Figure 5. (a) Visual comparison of H_4 dobdc (left), CORN-MOF-1 (Mg) (center), and Mg_2 (dobdc) (right) upon irradiation with UV light (230 nm), confirming the uniquely strong solid-state photoluminescence of CORN-MOF-1 (Mg). (b) Relative PL intensities of CORN-MOF-1 (Mg), Mg_2 (dobdc), and H_4 dobdc powder.

potentially because they are blocked by formates (see Section S15 for further discussion). Notably, CORN-MOF-1 (Mg) also (partially) degrades in MeOH and H_2O (SI Figures S79, S104), precluding the collection of reliable PL data in these solvents.

We evaluated the temperature-dependent PL using a gated intensified CCD camera with a 480 ps resolution (Figure 6df). Unlike common single-wavelength techniques such as timecorrelated single photon counting, this approach permits sensitive, direct detection of the full PL spectral evolution over the decay lifetime. 67 The strong emission of H₄dobdc in solution is quenched in the solid state (Figure 5). Intermolecular interactions evidently prevent the ESIPT mechanism, and rapid nonradiative decay dominates in solid H₄dobdc. This effect is manifested spectrally as a rapid transition into a weak, red-shifted state. The relative strength of this emission is significantly increased upon cooling (Figure 6d), indicating a suppression of a major nonradiative decay channel. This behavior is typical of excimers. ⁶⁸ The same basic behavior—fast conversion into a red-shifted excimer state—is observed in Mg₂(dobdc) powder as well (Figure 6e), indicating that the nonemissive nature of this MOF stems from rapid quenching into a dark excimer. The degree of redshift in the excimer is smaller in Mg₂(dobdc) than in H₄dobdc powder, indicating that intermolecular interactions are weaker in Mg₂(dobdc). This is likely due to the larger spacing between

linkers in the porous MOF compared to that in the dense H_4 dobdc solid (SI Figure S85). The excimer in Mg_2 (dobdc) also progressively blue-shifts on cooling. This effect has previously been observed in molecular films and is linked to the charge-transfer character of the excimer, 68 although its detailed origin remains unclear. No change in the prompt PL is observed at lower temperatures in either case. In contrast to both of these materials, the steady-state PL of CORN-MOF-1 (Mg) is essentially temperature-independent (Figure 6f), indicating that excimers do not play a major role in the photophysics of this material.

These observations are supported by an analysis of the decay lifetimes and detailed spectral evolutions (Figure 7). In THF (0.1 mM), H₄dobdc exhibits single-component exponential decay, consistent with the ESIPT mechanism (Figure 7a, see SI Figure S83 for other solvents). Both H₄dobdc powder and Mg₂(dobdc) demonstrate two-component exponential decay, with a faster and a slower time constant relative to the free linker (Figure 7a, Table S9). Consistent with our assignment above and with previous reports, ^{69–73} we assign the faster time constant to quenching of the $S_1 \rightarrow S_0$ emission, while the longer lifetime corresponds to emission from an excimer. The significantly shortened τ_1 in Mg₂(dobdc) and H₄dobdc powder explains why these samples do not visually appear bright under UV irradiation. This rapid decay is accompanied by a clear redshift and peak broadening, hallmarks of excimer formation in Mg₂(dobdc) and H₄dobdc powder (Figure 7b,c). This transition is better resolved in H₄dobdc powder than in Mg₂(dobdc) because the excimer formation process is slower in H₄dobdc than in Mg₂(dobdc) (Table S9). Excimer formation is common in pure organic films/powders, and the close packing of dobdc⁴⁻ linkers in Mg₂(dobdc) likely accounts for excimer formation in this material (SI Figure S85).^{24,74} Together, these photophysical data support that excimer formation quenches the PL of Mg₂(dobdc) and H₄dobdc powder and that dissolving H₄dobdc prevents excimer formation and allows for bright emission via an ESIPT mechanism.

Importantly, these features of excimer formation are entirely absent in the time-resolved PL spectra of CORN-MOF-1 (Mg; Figure 7d). Instead, we observe the same spectral shape from initial excitation out to longer time scales. In this sense, the spectral features of CORN-MOF-1 (Mg) most closely resemble those of dissolved H₄dobdc (Figure S82). Because CORN-MOF-1 (Mg) does not show any evidence of excimer formation, the spacing of linker molecules must be far enough apart on average for it to behave like a network of noninteracting linker molecules.³⁰ Thus, the emission mechanism of CORN-MOF-1 (Mg) is fundamentally different from all other reported H₂dobdc²⁻-based MOFs (Table S10). The nonsingle component decay kinetics reflect disorder in the environment of the emitting molecules, for instance due to defect or surface sites or variable coupling of the protonated linker molecules to formates within the pores. The PL decay curve for CORN-MOF-1 (Mg) can be equally fit to a stretched exponential function, indicating only a small degree of energetic disorder (Figure S86). However, anisotropy measurements show no resolvable energy transfer, in line with a lack of spectral diffusion during PL decay (SI Figure S87).

In addition to the rapid dynamics observed in these MOFs, blue-shifted emission was also detected on much longer time scales (SI Figures S86—S89). This emission is extremely weak and could possibly arise from upconversion in the MOFs. This

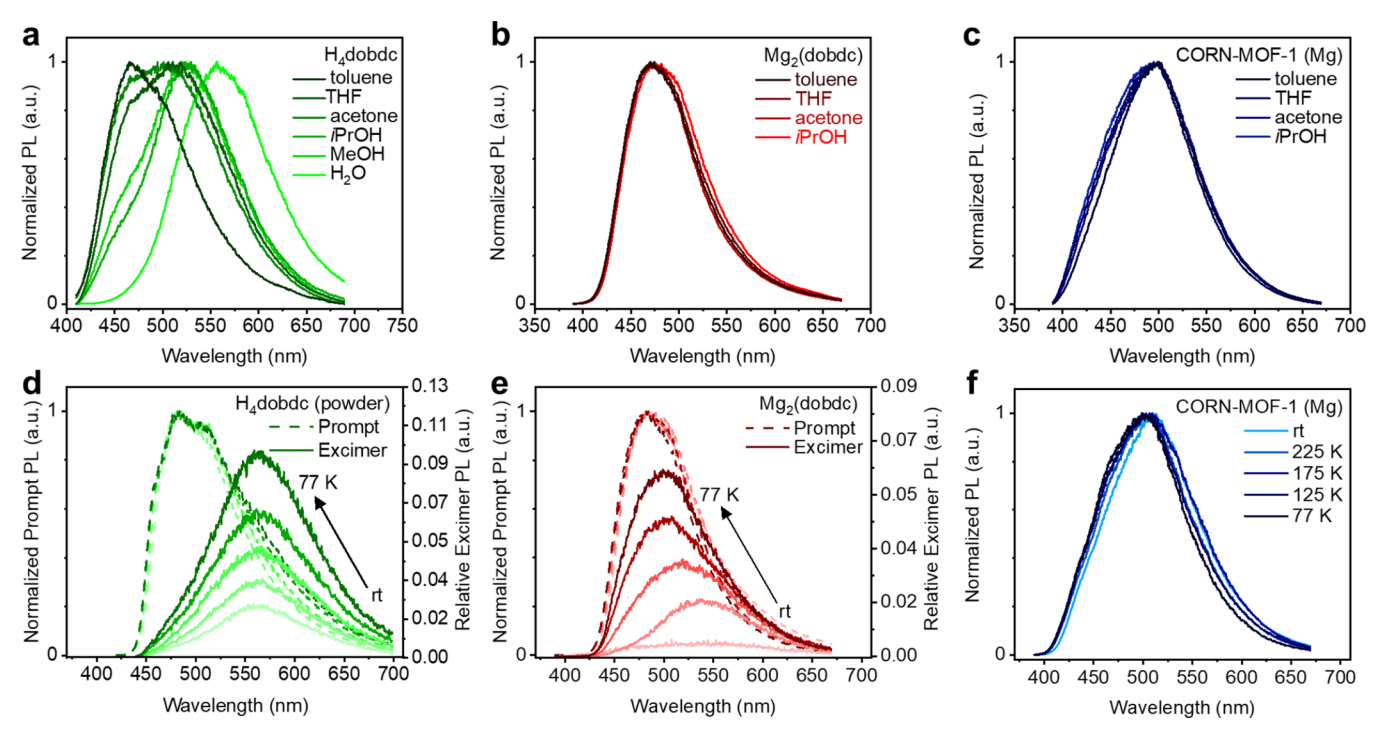


Figure 6. (a) Normalized, solvent-dependent PL spectra for H_4 dobdc (0.1 mM). Normalized, solvent-dependent PL spectra for suspensions (1 mg/mL) of (b) Mg_2 (dobdc) and (c) CORN-MOF-1 (Mg). (d) Spectral slices of the H_4 dobdc powder time-resolved PL capturing prompt emission (0 ns) and delayed excimer emission (5 ns) as a function of temperature. (e) Equivalent spectral slices of the Mg_2 (dobdc) time-resolved PL capturing prompt (0 ns) and delayed excimer (3 ns) emission. Temperature-dependent spectra for H_4 dobdc and Mg_2 (dobdc) are normalized to the prompt PL signal to demonstrate how the excimer PL intensity increases at a lower temperature due to the suppressed nonradiative decay. Time zeroes were set at the point of maximum PL intensity, and gate widths of 1 ns were used. (f) Normalized, temperature-dependent steady-state PL of CORN-MOF-1 (Mg). THF = tetrahydrofuran, iPrOH = isopropyl alcohol, and rt = room temperature (295 K).

phenomenon remains an active area of investigation in our groups.

Overall, these findings support that high-concentration synthesis provides a straightforward means to "turn on" the PL of $M_2(dobdc)$ derivatives. The rare combination of porosity and strong solid-state fluorescence in a Mg-based MOF (Table S10) makes CORN-MOF-1 (Mg) well-suited for applications in sensing and solid-state lighting that are not available to the parent $Mg_2(dobdc)$.

Conversion of CORN-MOF-1 to M_2 (dobdc). Our structural and photophysical studies thus far indicate that CORN-MOF-1 (Mg) is akin to partially formed Mg_2 (dobdc), with the linker phenol groups protonated and charge-balancing and/or coordinating formate groups in the pores. Previous studies have detected phases with H_2 dobdc²⁻ linkers during MOF self-assembly, but it remains unclear if they can generally be converted to the corresponding M_2 (dobdc) frameworks under synthetically relevant conditions. 12,34,39 We hypothesized that CORN-MOF-1 could potentially be converted into Mg_2 (dobdc) by treatment with an appropriate base to fully deprotonate the linkers, such as N_1N -dimethylamine generated from the decomposition of DMF (SI Section 4).

Consistent with this hypothesis, heating of CORN-MOF-1 (Mg) in DMF at 150 °C for 5 days allowed for its conversion into phase-pure Mg₂(dobdc), as confirmed by PXRD and a distinct color change from tan to yellow (Figure 8a,b). Conversion of large hexagonal plates of CORN-MOF-1 (Mg) into rods of Mg₂(dobdc) could also be monitored over time by SEM (Figure 8c-f), confirming that this process occurs as a solid-to-solid transformation (SI Figures S18, S19, and S22). After soaking in MeOH to remove soluble impurities, the

formate groups originally present in CORN-MOF-1 (Mg) were also absent in converted $Mg_2(dobdc)$ by ATR-IR (SI Figure S24). The overall process of synthesizing CORN-MOF-1 (Mg) and converting it into $Mg_2(dobdc)$ could be carried out on at least 10 mmol scale in good yield (4.23 g, 87% yield), in contrast to the traditional solvothermal synthesis of $Mg_2(dobdc)$, which failed on >1 g scale in our hands (SI Section 5).²²

After desolvation of the converted Mg₂(dobdc), its porosity was assessed using 77 K N₂ adsorption/desorption isotherms (Table 1, SI Figures S25 and S26). Intriguingly, its BET (1829 \pm 3 m²/g) and Langmuir (2060 \pm 2 m²/g) surface areas were found to be slightly higher than the BET (1743 m²/g)⁵⁴ and Langmuir (1957 \pm 2 m²/g)²⁵ surface areas reported for this material. Overall, these results suggest that the two-step synthesis of Mg₂(dobdc) has improved scalability and leads to a higher surface area MOF compared to the traditional solvothermal synthesis under dilute conditions.

Generalization to Other M_2 (dobdc) Variants. One of the most intriguing features of the M_2 (dobdc) family is the breadth of cations that can be incorporated into this framework. As such, we examined the generality of the formation of CORN-MOF-1 at high reaction concentrations with different metals (Figure 8). CORN-MOF-1 (Mn) also forms during attempted high-concentration syntheses of Mn_2 (dobdc) (Figure 8b, SI Figure S39, SI Section 7). This material could be converted into Mn_2 (dobdc) by heating in DMF (Figure 8b, SI Section 8). Consistent with the results observed for the Mg analogue, the BET surface area of Mn_2 (dobdc) prepared from CORN-MOF-1 (Mn) was higher (1165 \pm 9 m²/g, Table 1, SI Figure S56 and S57) than that

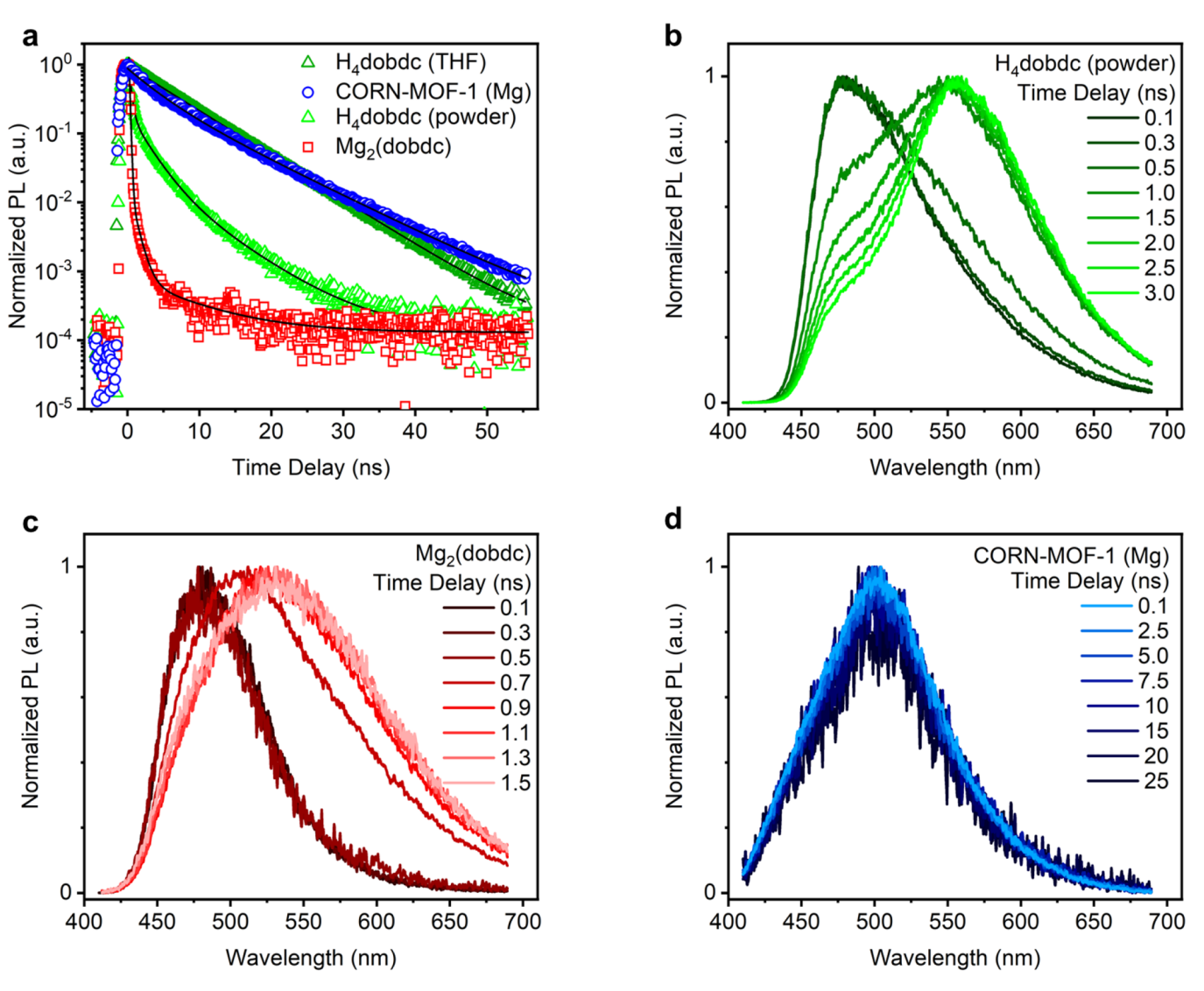


Figure 7. (a) PL decay curves for 0.1 mM H_4 dobdc in THF (dark-green triangles), CORN-MOF-1 (Mg) powder (blue circles), H_4 dobdc powder (light green triangles), and Mg_2 (dobdc) powder (red squares). Decay curves were extracted by integration over the entire PL spectrum. (b) Spectral evolution of H_4 dobdc powder within the first 3 ns. (c) Spectral evolution of Mg_2 (dobdc) within the first 1.5 ns. The excimer formation is near the 1 ns resolution of the ICCD. (d) Spectral evolution of CORN-MOF-1 (Mg) within the first 25 ns.

reported previously for this MOF ($1102 \text{ m}^2/\text{g}$).²² As previous studies into the mechanism of $M_2(\text{dobdc})$ formation have focused on the Mg, Co, Ni, and Zn congeners, 12,39,44,52 this represents the first experimental evidence that $Mn_2(\text{dobdc})$ likely also forms via stepwise deprotonation of the linker.

Carrying out the synthesis of Ni₂(dobdc) at high reaction concentrations consistently produced a mixture of CORN-MOF-1 (Ni) and Ni₂(dobdc) (Figure 8b, SI Figure S63, SI Section 10). The observation of Ni₂(dobdc) even at concentrations as high as 1.5 M is likely due to the poor reversibility of Ni₂(dobdc) formation, which arises from the strong Ni–O bonds comprising this MOF. Once again, phasepure Ni₂(dobdc) could be prepared on a multigram scale from the mixture containing CORN-MOF-1 (Ni) (Figure 8b, SI Section 11) with a higher BET surface area (1270 \pm 1, Table 1, SI Figures S71 and 72) than material prepared by the traditional solvothermal route (1218 $\rm m^2/g).^{54}$ Ni₂(dobdc) prepared via CORN-MOF-1 (Ni) also exhibits better-defined crystallites by SEM compared to the material prepared under traditional conditions (SI Figure S68). Overall, these findings

suggest that the phase change to CORN-MOF-1 at higher reaction concentrations is general among $M_2(\mbox{dobdc})$ frameworks. The large scales at which these two-step syntheses furnish high-quality $M_2(\mbox{dobdc})$ without the requirement for specialized equipment gives this method an edge over state-of-the-art alternatives, such as mechanochemical syntheses that require ball mills. 38,44,78,79

A break in this trend was observed for the Zn congener (SI Section 13). Although CORN-MOF-1 (Zn) was not observed, its attempted synthesis at a linker concentration of 1.0 M yielded the known one-dimensional polymer Zn₂(H₂dobdc) instead (SI Figure S77). 44,46 Previous studies suggest that this material is a kinetic intermediate formed en route to Zn₂(dobdc) under mechanochemical conditions. 44 Thus, its formation under conditions similar to those for CORN-MOF-1 (Mg, Mn, Ni) further supports that the CORN-MOF-1 congeners are formed during the solvothermal syntheses of the corresponding M₂(dobdc) analogues. CORN-MOF-1 (Zn) is likely not formed due to the lability of Zn–O bonds compared to Mg–O, Mn–O, and Ni–O bonds, and the flexibility of Zn

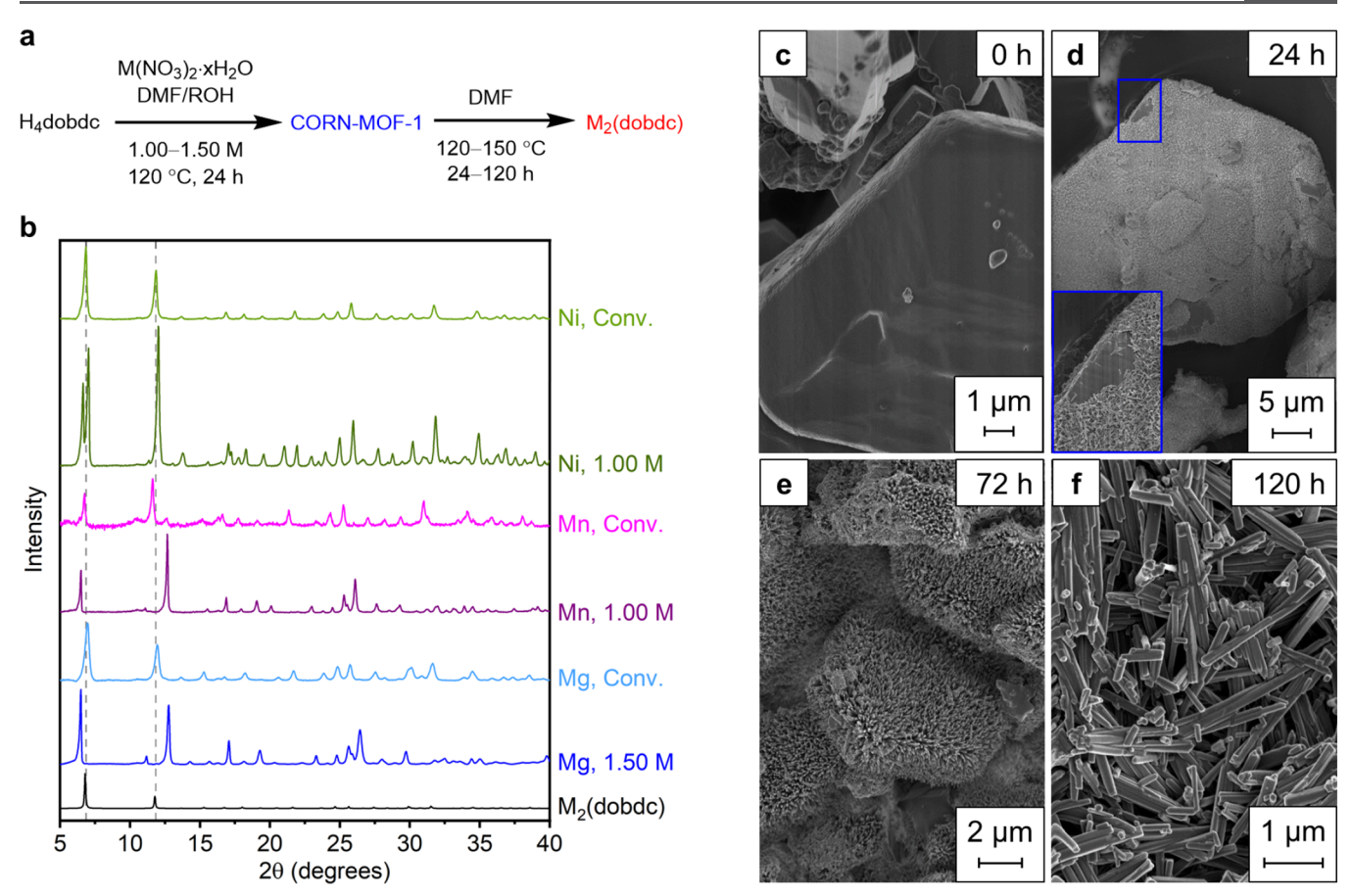


Figure 8. (a) Synthesis of Mg, Mn, and Ni analogues of CORN-MOF-1, and M_2 (dobdc) converted from the corresponding CORN-MOF-1 analogues. (b) PXRD patterns of CORN-MOF-1 (Mg, Mn, and Ni) and the converted M_2 (dobdc) (M = Mg, Mn, and Ni) analogues. SEM images of the conversion of CORN-MOF-1 (Mg) hexagonal plates to M_2 (dobdc) rods by heating in DMF at 150 °C after (c) 0, (d) 24, (e) 72, and (f) 120 h. R = alkyl, H.

Table 1. BET Surface Areas of $M_2(dobdc)$ Samples Prepared from the Corresponding CORN-MOF-1 Analogues

M ₂ (dobdc)	BET surface area	BET surface area (lit.)
Mg	1829 ± 3	1743 ⁵⁴
Mn	1165 ± 9	1102 ²²
Ni	1270 ± 1	1218 ⁵⁴

coordination complexes. The observed 1D polymer $\mathrm{Zn_2}(\mathrm{H_2}\mathrm{dobdc})$, which has an octahedral geometry with two weakly bound solvent molecules, is likely more stable than the analogous CORN-MOF-1 phase.

CONCLUSIONS

Herein, we have demonstrated that simply increasing the concentration of the solvothermal synthesis of $M_2(dobdc)$ analogues (M = Mg, Mn, Ni) up to 150-fold leads to a new phase, CORN-MOF-1, with protonated phenol groups and charge-balancing or coordinated formate groups in the pores. This finding supports previous findings that stepwise linker deprotonation occurs during the self-assembly of $M_2(dobdc)$ materials 12,39,44,52 and implicates formate as a noninnocent species during MOF formation in formamide solvents. Critically, CORN-MOF-1 (Mg) is highly photoluminescent in the solid state, whereas closely related H_4 dobdc and $Mg_2(dobdc)$ are only weakly emissive, which photophysical studies confirm is due to the suppression of dark excimer

formation in CORN-MOF-1 (Mg). Notably, CORN-MOF-1 (Mg) is the first framework based on the H₂dobdc²⁻ linker that is not proposed to emit via an ESIPT pathway, broadening the scope of photophysical properties that can be unlocked by using these materials. Together, these findings support that high-concentration synthesis represents an underutilized method to gain mechanistic insight into the pathways of MOF self-assembly and to identify new phases with distinct (photo)physical properties from known materials.

In addition, we have shown that kinetic phases formed at high concentrations can be converted into the known thermodynamic $M_2(dobdc)$ materials. The produced frameworks are highly crystalline and possess BET surface areas that are consistently higher than those obtained by a traditional solvothermal synthesis. This novel two-step synthetic approach is amenable to the multigram-scale synthesis of $M_2(dobdc)$ (M = Mg, Mn, Ni) materials without the need for specialized equipment.

We anticipate that these findings will guide the development of high-concentration syntheses of other MOFs. Two desirable outcomes can be envisaged: the formation of the same phase as the reaction concentration is increased, which allows for MOFs to be prepared with significantly reduced solvent use or the formation of new phases with distinct properties from known combinations of linkers and metal salts. In the latter case, changing the concentration of a MOF synthesis is much simpler than evaluating dozens of conditions to produce a new

MOF phase from a given linker-metal combination. As such, high-concentration solvothermal synthesis should be added to the growing lexicon of methods available for the synthesis of MOFs and other metal—organic materials. Future work will focus on growing high-quality single crystals of CORN-MOF-1 variants to enable their structure determination and investigating the high-concentration solvothermal syntheses of other MOFs.

■ EXPERIMENTAL SECTION

Characterization Details. Full details of all measurements are provided in the SI. ATR-IR spectra were collected on a Bruker Tensor II spectrometer equipped with a diamond ATR attachment. Surface area data were collected on either a Micromeritics ASAP 2020 or a Micromeritics 3Flex gas sorption analyzer using ultrapure N₂ (99.999%) and a liquid N₂ bath. Laboratory PXRD data were collected on a Rigaku Ultima IV diffractometer equipped with a Cu $\rm K_{\alpha}$ source ($\lambda=1.5406~\rm \mathring{A})$. $^{\rm 1}H$ NMR data were collected on a Bruker INOVA 500 MHz spectrometer and are referenced to the residual solvent. Thermogravimetric analysis (TGA) experiments were conducted by using a TA Instruments TGA Q500 under a flow of dry N₂ (60 mL/min). Masses are uncorrected for buoyancy effects. Differential scanning calorimetry (DSC) measurements were conducted using a TA Instruments Q1000 modulated differential scanning calorimeter (MDSC) under an atmosphere of dry He.

SSNMR experiments were performed at a field strength of 9.4 T (400 MHz for ¹H) using a Bruker AVANCE I console with a 2.5 mm MAS probe. All SSNMR experiments were performed at a MAS rate of 25 kHz. ¹H NMR spectra were recorded via a simple pulse-acquisition sequence with the recycle delay adjusted to yield quantitative data. A ¹H probe background spectrum was also recorded and subtracted from the data to give the final spectra. ¹³C NMR spectra were obtained by cross-polarization (CP) from ¹H with a contact time of 1 ms (unless otherwise specified) and with continuous-wave ¹H decoupling. NMR spectra were referenced to adamantane at 1.8 ppm for ¹H and at 38.5 ppm for ¹³C (left-hand resonance).

SEM images were collected at 1.0 kV using a Zeiss Gemini 500 Scanning Electron Microscope. The powder samples were immobilized on carbon tape mounted on an aluminum stub. The samples were blown using compressed air to remove excess material not stuck to the tape and then coated with a carbon layer on samples dried at 30 °C prior to analysis.

Detailed procedures for PL and TEM measurements as well as DFT calculations are provided in the SI.

Representative Synthesis of CORN-MOF-1 (Mg). A 75 mL screw-cap high-pressure flask equipped with a stir bar was charged with Mg(NO₃)₂•6H₂O (9.62 g, 37.5 mmol, 2.50 equiv), H₄dobdc (2.97 g, 15.0 mmol, 1.00 equiv), DMF (9.0 mL), EtOH (0.5 mL), and water (0.5 mL). The flask was sealed and placed in a silicone oil bath, and the reaction mixture was heated to 120 °C while being vigorously stirred (1000 rpm). The reaction mixture was stirred at 120 °C for 24 h. At this time, the reaction mixture was cooled to room temperature and filtered. The resulting solid was washed thoroughly with DMF (100 mL) and MeOH (100 mL). Drying under a vacuum yielded CORN-MOF-1 (Mg) as a tan solid (~6.6 g).

ASSOCIATED CONTENT

Supporting Information

The Supporting Information is available free of charge at https://pubs.acs.org/doi/10.1021/acs.chemmater.3c02121.

Detailed synthetic procedures as well as spectroscopic, crystallographic, and computational data (PDF)

AUTHOR INFORMATION

Corresponding Author

Phillip J. Milner — Department of Chemistry and Chemical Biology, Cornell University, Ithaca, New York 14850, United States; orcid.org/0000-0002-2618-013X; Email: pjm347@cornell.edu

Authors

Arjun Halder – Department of Chemistry and Chemical Biology, Cornell University, Ithaca, New York 14850, United States

David C. Bain – Department of Chemistry and Chemical Biology, Cornell University, Ithaca, New York 14850, United States

Tristan A. Pitt – Department of Chemistry and Chemical Biology, Cornell University, Ithaca, New York 14850, United States

Zixiao Shi — School of Applied Engineering and Physics, Cornell University, Ithaca, New York 14850, United States

Julia Oktawiec – Department of Chemistry, Northwestern University, Evanston, Illinois 60208, United States

Jung-Hoon Lee — Computational Science Research Center, Korea Institute of Science and Technology, Seoul 02792, Republic of Korea; Oorcid.org/0000-0002-2983-678X

Stavrini Tsangari – Department of Chemistry and Chemical Biology, Cornell University, Ithaca, New York 14850, United States

Marcus Ng — Department of Chemistry and Chemical Biology, Cornell University, Ithaca, New York 14850, United States José J. Fuentes-Rivera — Department of Chemistry and Chemical Biology, Cornell University, Ithaca, New York 14850, United States; orcid.org/0000-0002-8861-6752

Alexander C. Forse – Department of Chemistry, University of Cambridge, Cambridge CB2 1EW, United Kingdom;
orcid.org/0000-0001-9592-9821

Tomče Runčevski – Department of Chemistry, Southern Methodist University, Dallas, Texas 75275, United States

David A. Muller — School of Applied Engineering and Physics, Cornell University, Ithaca, New York 14850, United States; Kavli institute at Cornell for Nanoscale Science, Cornell University, Ithaca, New York 14850, United States

Andrew J. Musser — Department of Chemistry and Chemical Biology, Cornell University, Ithaca, New York 14850, United States; o orcid.org/0000-0002-4600-6606

Complete contact information is available at: https://pubs.acs.org/10.1021/acs.chemmater.3c02121

Funding

The development of scalable routes to prepare M₂(dobdc) analogues was supported by the National Institute of General Medical Sciences of the National Institutes of Health under award number R35GM138165 (A.H., T.A.P., M.N., J.J.F.-R., P.J.M.). The content is solely the responsibility of the authors and does not necessarily represent the official views of the National Institutes of Health. We acknowledge the support of a Camille Dreyfus Teacher-Scholar Award to P.J.M. (TC-23–048). Further support was provided by a Cornell University College of Arts and Sciences New Frontiers Grant awarded to P.J.M. and A.J.M. A.J.M. acknowledges the donors of the American Chemical Society Petroleum Research Fund for partial support of this research. J.O. was supported by the National Institute of General Medical Sciences under award F32GM143925. J.-H.L. was supported by the KIST Institu-

tional Program (Project No. 2E32531) and the National Center for Materials Research Data (NCMRD) (Project No. 2021M3A7C2089739) and the program of Future Hydrogen Original Technology Development (Project No. 2021M3I3A1083946), through the National Research Foundation of Korea (NRF), funded by the Ministry of Science and ICT. Computational resources provided by KISTI Supercomputing Center (Project No. KSC-2020-CRE-0361). T.R. acknowledges the support of the Welch Foundation (Grant No.: N-2012-20220331). We acknowledge support from a UKRI Future Leaders Fellowship to A.C.F. (MR/T043024/1). Z.S. and D.A.M. acknowledge support from the Center for Alkaline-Based Energy Solutions (CABES), an Energy Frontier Research Center funded by the U.S. Department of Energy, Office of Science, Basic Energy Sciences, under Award DE-SC0019445. This work made use of the Cornell Center for Materials Research Shared Facilities, which are supported through the NSF MRSEC program (DMR-1719875). ¹H NMR data were collected on a Bruker INOVA 500 MHz spectrometer that was purchased with support from the NSF (CHE-1531632).

Notes

The authors declare the following competing financial interest(s): P.J.M. is listed as a co-inventor on several patents related to the applications of MOFs.

ACKNOWLEDGMENTS

We thank Drs. Craig Brown and Benjamin Trump (NIST) for assistance with analyzing PXRD data and helpful discussions. We thank Kaitlyn Keasler (Cornell University) for helpful discussions and for reproducing the synthesis of CORN-MOF-1 (Mg).

REFERENCES

- (1) Bavykina, A.; Kolobov, N.; Khan, I. S.; Bau, J. A.; Ramirez, A.; Gascon, J. Metal-Organic Frameworks in Heterogeneous Catalysis: Recent Progress, New Trends, and Future Perspectives. *Chem. Rev.* **2020**, *120* (16), 8468–8535.
- (2) Sun, Y.; Zheng, L.; Yang, Y.; Qian, X.; Fu, T.; Li, X.; Yang, Z.; Yan, H.; Cui, C.; Tan, W. Metal—Organic Framework Nanocarriers for Drug Delivery in Biomedical Applications. *Nano-Micro Lett.* **2020**, *12* (1), 103.
- (3) Furukawa, H.; Cordova, K. E.; O'Keeffe, M.; Yaghi, O. M. The Chemistry and Applications of Metal-Organic Frameworks. *Science* **2013**, *341* (6149), 1230444–1230444.
- (4) Li, J.-R.; Sculley, J.; Zhou, H.-C. Metal-Organic Frameworks for Separations. *Chem. Rev.* **2012**, *112* (2), 869–932.
- (5) Gong, X.; Noh, H.; Gianneschi, N. C.; Farha, O. K. Interrogating Kinetic versus Thermodynamic Topologies of Metal—Organic Frameworks via Combined Transmission Electron Microscopy and X-Ray Diffraction Analysis. *J. Am. Chem. Soc.* **2019**, *141* (15), 6146–6151.
- (6) Pang, J.; Yuan, S.; Qin, J.; Liu, C.; Lollar, C.; Wu, M.; Yuan, D.; Zhou, H.-C.; Hong, M. Control the Structure of Zr-Tetracarboxylate Frameworks through Steric Tuning. *J. Am. Chem. Soc.* **2017**, *139* (46), 16939–16945.
- (7) Ma, J.; Tran, L. D.; Matzger, A. J. Toward Topology Prediction in Zr-Based Microporous Coordination Polymers: The Role of Linker Geometry and Flexibility. *Cryst. Growth Des.* **2016**, *16* (7), 4148–4153
- (8) Stock, N.; Biswas, S. Synthesis of Metal-Organic Frameworks (MOFs): Routes to Various MOF Topologies, Morphologies, and Composites. *Chem. Rev.* **2012**, *112* (2), 933–969.

- (9) Van Vleet, M. J.; Weng, T.; Li, X.; Schmidt, J. R. In Situ, Time-Resolved, and Mechanistic Studies of Metal-Organic Framework Nucleation and Growth. *Chem. Rev.* **2018**, *118* (7), 3681–3721.
- (10) Yuan, S.; Qin, J.-S.; Li, J.; Huang, L.; Feng, L.; Fang, Y.; Lollar, C.; Pang, J.; Zhang, L.; Sun, D.; Alsalme, A.; Cagin, T.; Zhou, H.-C. Retrosynthesis of Multi-Component Metal—organic Frameworks. *Nat. Commun.* **2018**, *9* (1), 808.
- (11) Ryu, U.; Jee, S.; Rao, P. C.; Shin, J.; Ko, C.; Yoon, M.; Park, K. S.; Choi, K. M. Recent Advances in Process Engineering and Upcoming Applications of Metal—Organic Frameworks. *Coord. Chem. Rev.* **2021**, *426*, No. 213544.
- (12) Du Bois, D. R.; Wright, K. R.; Bellas, M. K.; Wiesner, N.; Matzger, A. J. Linker Deprotonation and Structural Evolution on the Pathway to MOF-74. *Inorg. Chem.* **2022**, *61* (11), 4550–4554.
- (13) Du Bois, D. R.; Matzger, A. J. Metal-Organic Framework Seeding to Drive Phase Selection and Overcome Synthesis Limitations. *Cryst. Growth Des.* **2022**, 22 (11), 6379–6383.
- (14) Li, Q.; Gies, J.; Yu, X.; Gu, Y.; Terfort, A.; Kind, M. Concentration-Dependent Seeding as a Strategy for Fabrication of Densely Packed Surface-Mounted Metal-Organic Frameworks (SURMOF) Layers. Chem.—Eur. J. 2020, 26 (23), 5185–5189.
- (15) McKinstry, C.; Cussen, E. J.; Fletcher, A. J.; Patwardhan, S. V.; Sefcik, J. Effect of Synthesis Conditions on Formation Pathways of Metal Organic Framework (MOF-5) Crystals. *Cryst. Growth Des.* **2013**, *13* (12), 5481–5486.
- (16) Forster, P. M.; Stock, N.; Cheetham, A. K. A High-Throughput Investigation of the Role of PH, Temperature, Concentration, and Time on the Synthesis of Hybrid Inorganic-Organic Materials. *Angew. Chem., Int. Ed.* **2005**, 44 (46), 7608–7611.
- (17) Jerozal, R.; Pitt, T.; MacMillan, S.; Milner, P. High-Concentration Self-Assembly of Zirconium- and Hafnium-Based Metal-Organic Materials. *J. Am. Chem. Soc.* **2023**, *145* (24), 13273–13283.
- (18) Siegelman, R. L.; McDonald, T. M.; Gonzalez, M. I.; Martell, J. D.; Milner, P. J.; Mason, J. A.; Berger, A. H.; Bhown, A. S.; Long, J. R. Controlling Cooperative CO₂ Adsorption in Diamine-Appended Mg₂(dobpdc) Metal—Organic Frameworks. *J. Am. Chem. Soc.* **2017**, 139 (30), 10526–10538.
- (19) Furukawa, H.; Gándara, F.; Zhang, Y.-B.; Jiang, J.; Queen, W. L.; Hudson, M. R.; Yaghi, O. M. Water Adsorption in Porous Metal—Organic Frameworks and Related Materials. *J. Am. Chem. Soc.* **2014**, 136 (11), 4369–4381.
- (20) Morelli Venturi, D.; Campana, F.; Marmottini, F.; Costantino, F.; Vaccaro, L. Extensive Screening of Green Solvents for Safe and Sustainable UiO-66 Synthesis. ACS Sustainable Chem. Eng. 2020, 8 (46), 17154–17164.
- (21) Xiao, T.; Liu, D. The Most Advanced Synthesis and a Wide Range of Applications of MOF-74 and Its Derivatives. *Microporous Mesoporous Mater.* **2019**, 283, 88–103.
- (22) Caskey, S. R.; Wong-Foy, A. G.; Matzger, A. J. Dramatic Tuning of Carbon Dioxide Uptake via Metal Substitution in a Coordination Polymer with Cylindrical Pores. *J. Am. Chem. Soc.* **2008**, 130 (33), 10870–10871.
- (23) Dietzel, P. D. C.; Panella, B.; Hirscher, M.; Blom, R.; Fjellvåg, H. Hydrogen Adsorption in a Nickel Based Coordination Polymer with Open Metal Sites in the Cylindrical Cavities of the desolvated Framework. *Chem. Commun.* **2006**, 2006 (9), 959.
- (24) Rosi, N. L.; Kim, J.; Eddaoudi, M.; Chen, B.; O'Keeffe, M.; Yaghi, O. M. Rod Packings and Metal–Organic Frameworks Constructed from Rod-Shaped Secondary Building Units. *J. Am. Chem. Soc.* **2005**, 127 (5), 1504–1518.
- (25) Queen, W. L.; Hudson, M. R.; Bloch, E. D.; Mason, J. A.; Gonzalez, M. I.; Lee, J. S.; Gygi, D.; Howe, J. D.; Lee, K.; Darwish, T. A.; James, M.; Peterson, V. K.; Teat, S. J.; Smit, B.; Neaton, J. B.; Long, J. R.; Brown, C. M. Comprehensive Study of Carbon Dioxide Adsorption in the Metal—Organic Frameworks M₂(dobdc) (M= Mg, Mn, Fe, Co, Ni, Cu, Zn). *Chem. Sci.* **2014**, 5 (12), 4569–4581.
- (26) Zick, M. E.; Lee, J.-H.; Gonzalez, M. I.; Velasquez, E. O.; Uliana, A. A.; Kim, J.; Long, J. R.; Milner, P. J. Fluoroarene

- Separations in Metal-Organic Frameworks with Two Proximal Mg²⁺ Coordination Sites. *J. Am. Chem. Soc.* **2021**, *143*, 1948–1958.
- (27) Xiao, D. J.; Bloch, E. D.; Mason, J. A.; Queen, W. L.; Hudson, M. R.; Planas, N.; Borycz, J.; Dzubak, A. L.; Verma, P.; Lee, K.; Bonino, F.; Crocellà, V.; Yano, J.; Bordiga, S.; Truhlar, D. G.; Gagliardi, L.; Brown, C. M.; Long, J. R. Oxidation of Ethane to Ethanol by N_2O in a Metal—Organic Framework with coordinatively Unsaturated Iron(II) Sites. *Nat. Chem.* **2014**, *6* (7), 590–595.
- (28) Calleja, G.; Sanz, R.; Orcajo, G.; Briones, D.; Leo, P.; Martínez, F. Copper-Based MOF-74 Material as Effective Acid Catalyst in Friedel—Crafts Acylation of Anisole. *Catal. Today* **2014**, 227, 130—137.
- (29) Huang, P.; Liu, Y.; Karmakar, A.; Yang, Q.; Li, J.; Wu, F.-Y.; Deng, K.-Y. Tuning the Excited-State Intramolecular Proton Transfer (ESIPT)-Based Luminescence of Metal—Organic Frameworks by Metal Nodes toward Versatile photoluminescent Applications. *Dalton Trans.* **2021**, *50* (20), *6901*–*6912*.
- (30) Douvali, A.; Tsipis, A. C.; Eliseeva, S. V.; Petoud, S.; Papaefstathiou, G. S.; Malliakas, C. D.; Papadas, I.; Armatas, G. S.; Margiolaki, I.; Kanatzidis, M. G.; Lazarides, T.; Manos, M. J. Turn-On Luminescence Sensing and Real-Time Detection of Traces of Water in Organic Solvents by a Flexible Metal-Organic Framework. *Angew. Chem.* 2015, 127 (5), 1671–1676.
- (31) Jayaramulu, K.; Kanoo, P.; George, S. J.; Maji, T. K. Tunable Emission from a Porous Metal—Organic Framework by Employing an Excited-State Intramolecular Proton Transfer Responsive Ligand. *Chem. Commun.* **2010**, *46* (42), 7906.
- (32) Henkelis, S. E.; McCormick, L. J.; Cordes, D. B.; Slawin, A. M. Z.; Morris, R. E. Synthesis and Crystallographic Characterisation of Mg(H₂Dhtp)(H₂O)₅·H₂O. *Inorg. Chem. Commun.* **2016**, 65, 21–23.
- (33) Cheansirisomboon, A.; Salinas-Uber, J.; Massera, C.; Roubeau, O.; Youngme, S.; Gamez, P. One-Pot Multiple Metal-Organic Framework Formation: Concomitant Generation of Structural Isomers or of Drastically Distinct Materials: One-Pot Multiple Metal-Organic Framework Formation. *Eur. J. Inorg. Chem.* **2014**, 2014 (26), 4385–4393.
- (34) Dietzel, P. D. C.; Blom, R.; Fjellvåg, H. Base-Induced Formation of Two Magnesium Metal-Organic Framework Compounds with a Bifunctional Tetratopic Ligand. *Eur. J. Inorg. Chem.* **2008**, 2008 (23), 3624–3632.
- (35) Douvali, A.; Papaefstathiou, G. S.; Gullo, M. P.; Barbieri, A.; Tsipis, A. C.; Malliakas, C. D.; Kanatzidis, M. G.; Papadas, I.; Armatas, G. S.; Hatzidimitriou, A. G.; Lazarides, T.; Manos, M. J. Alkaline Earth Metal Ion/Dihydroxy—Terephthalate MOFs: Structural Diversity and Unusual Luminescent Properties. *Inorg. Chem.* **2015**, *54* (12), 5813–5826.
- (36) Henkelis, S. E.; Rademacher, D.; Vogel, D. J.; Valdez, N. R.; Rodriguez, M. A.; Rohwer, L. E. S.; Nenoff, T. M. Luminescent Properties of dobdc Containing MOFs: The Role of Free Hydroxyls. ACS Appl. Mater. Interfaces 2020, 12 (20), 22845–22852.
- (37) Gao, Q.; Jiang, F.-L.; Wu, M.-Y.; Huang, Y.-G.; Wei, W.; Zhang, Q.-F.; Hong, M.-C. Crystal Structures, Topological Analyses, and Magnetic Properties of Manganese-Dihydroxyterephthalate Complexes. *Aust. J. Chem.* **2010**, *63* (2), 286.
- (38) Ayoub, G.; Karadeniz, B.; Howarth, A. J.; Farha, O. K.; Đilović, I.; Germann, L. S.; Dinnebier, R. E.; Užarević, K.; Friščić, T. Rational Synthesis of Mixed-Metal Microporous Metal—Organic Frameworks with Controlled Composition Using Mechanochemistry. *Chem. Mater.* **2019**, *31* (15), 5494–5501.
- (39) Rosnes, M. H.; Mathieson, J. S.; Törnroos, K. W.; Johnsen, R. E.; Cronin, L.; Dietzel, P. D. C. Electrospray Mass Spectrometry Investigation into the Formation of CPO-27. *Cryst. Growth Des.* **2019**, 19 (4), 2089–2096.
- (40) Flores, L. S.; Alcântara, S. P.; de Lima, G. C. G.; Yoshida, M. I.; Corrêa, C. C. Vibrational Analysis and Crystal Structure of Two New 1D Cu^{II} and Co^{II} Coordination Polymers, Involving the Ligands 2,5-Dihydroxyterephthalate and Glutarate. *Vib. Spectrosc.* **2016**, *86*, 302–310.

- (41) Rosa, I. M. L.; Costa, M. C. S.; Vitto, B. S.; Amorim, L.; Correa, C. C.; Pinheiro, C. B.; Doriguetto, A. C. Influence of Synthetic Methods in the Structure and Dimensionality of Coordination Polymers. *Cryst. Growth Des.* **2016**, *16* (3), 1606–1616.
- (42) Gheorghe, A.; Imaz, I.; van der Vlugt, J. I.; Maspoch, D.; Tanase, S. Tuning the Supramolecular Isomerism of MOF-74 by Controlling the Synthesis Conditions. *Dalton Trans.* **2019**, *48* (27), 10043–10050.
- (43) Kim, D.; Coskun, A. Template-Directed Approach Towards the Realization of Ordered Heterogeneity in Bimetallic Metal-Organic Frameworks. *Angew. Chem., Int. Ed.* **2017**, *56* (18), 5071–5076.
- (44) Julien, P. A.; Užarević, K.; Katsenis, A. D.; Kimber, S. A. J.; Wang, T.; Farha, O. K.; Zhang, Y.; Casaban, J.; Germann, L. S.; Etter, M.; Dinnebier, R. E.; James, S. L.; Halasz, I.; Friščić, T. *In Situ* Monitoring and Mechanism of the Mechanochemical Formation of a Microporous MOF-74 Framework. *J. Am. Chem. Soc.* 2016, 138 (9), 2929–2932.
- (45) Luo, F.; Yan, C.; Dang, L.; Krishna, R.; Zhou, W.; Wu, H.; Dong, X.; Han, Y.; Hu, T.-L.; O'Keeffe, M.; Wang, L.; Luo, M.; Lin, R.-B.; Chen, B. UTSA-74: A MOF-74 Isomer with Two Accessible Binding Sites per Metal Center for Highly Selective Gas Separation. *J. Am. Chem. Soc.* **2016**, *138* (17), 5678–5684.
- (46) Ghermani, N. E.; Morgant, G.; d'Angelo, J.; Desmaële, D.; Fraisse, B.; Bonhomme, F.; Dichi, E.; Sgahier, M. Covalently Bonded Infinite Zigzag Chain Structure in a Novel Zn(II) Complex of 2,5-Dihydroxy-1,6-Benzenedicarboxylic Acid. *Polyhedron* **2007**, 26 (12), 2880–2884.
- (47) Zhao, Y.; Shao, L.; Li, L.; Wang, S.; Song, G.; Gao, Z.; Zhang, X.; Wang, T.; Li, Y.; Zhang, L.; Li, W.; Meng, F.; Fu, Y. Novel Zinc-Based Infinite Coordination Polymer for Highly Selective Ammonia Gas Sensing at Room Temperature. *BCSJ.* **2020**, *93* (9), 1070–1073.
- (48) Lefton, J. B.; Pekar, K. B.; Haris, U.; Zick, M. E.; Milner, P. J.; Lippert, A. R.; Pejov, L.; Runčevski, T. Defect Formation and Amorphization of Zn-MOF-74 Crystals by Post-Synthetic Interactions with Bidentate Adsorbates. *J. Mater. Chem. A* **2021**, *9*, 19698–19704.
- (49) Albuquerque, G. H.; Fitzmorris, R. C.; Ahmadi, M.; Wannenmacher, N.; Thallapally, P. K.; McGrail, B. P.; Herman, G. S. Gas—Liquid Segmented Flow Microwave-Assisted Synthesis of MOF-74(Ni) under Moderate Pressures. *CrystEngComm* **2015**, *17* (29), 5502—5510.
- (50) El Osta, R.; Feyand, M.; Stock, N.; Millange, F.; Walton, R. I. Crystallisation Kinetics of Metal Organic Frameworks From *in Situ* Time-Resolved X-Ray Diffraction. *Powder Diffr.* **2013**, 28 (S2), S256—S275.
- (51) Haque, E.; Jhung, S. H. Synthesis of Isostructural Metal—Organic Frameworks, CPO-27s, with Ultrasound, Microwave, and Conventional Heating: Effect of Synthesis Methods and Metal Ions. *Chem. Eng. J.* **2011**, *173* (3), 866–872.
- (52) Beamish-Cook, J.; Shankland, K.; Murray, C. A.; Vaqueiro, P. Insights into the Mechanochemical Synthesis of MOF-74. *Cryst. Growth Des.* **2021**, *21* (5), 3047–3055.
- (53) Mason, J. A.; Veenstra, M.; Long, J. R. Evaluating Metal—Organic Frameworks for Natural Gas Storage. *Chem. Sci.* **2014**, 5 (1), 32–51.
- (54) Dietzel, P. D. C.; Georgiev, P. A.; Eckert, J.; Blom, R.; Strässle, T.; Unruh, T. Interaction of Hydrogen with Accessible Metal Sites in the Metal—Organic Frameworks $M_2(dhtp)$ (CPO-27-M; M = Ni, Co, Mg). Chem. Commun. **2010**, 46 (27), 4962.
- (55) Remy, T.; Peter, S. A.; Van der Perre, S.; Valvekens, P.; De Vos, D. E.; Baron, G. V.; Denayer, J. F. M. Selective Dynamic CO₂ Separations on Mg-MOF-74 at Low Pressures: A Detailed Comparison with 13X. *J. Phys. Chem. C* **2013**, *117* (18), 9301–9310. (56) Dietzel, P. D. C.; Johnsen, R. E.; Blom, R.; Fjellvåg, H. Structural Changes and coordinatively Unsaturated Metal Atoms on
- Structural Changes and coordinatively Unsaturated Metal Atoms on Dehydration of Honeycomb Analogous Microporous Metal—Organic Frameworks. *Chem.—Eur. J.* **2008**, 14 (8), 2389–2397.
- (57) Milner, P. J.; Martell, J. D.; Siegelman, R. L.; Gygi, D.; Weston, S. C.; Long, J. R. Overcoming Double-Step CO₂ Adsorption and

Minimizing Water Co-Adsorption in Bulky Diamine-Appended Variants of Mg ₂ (Dobpdc). *Chem. Sci.* **2018**, 9 (1), 160–174.

- (58) Moon, H.-S.; Moon, J.-H.; Chun, D. H.; Park, Y. C.; Yun, Y. N.; Sohail, M.; Baek, K.; Kim, H. Synthesis of [Mg₂ (dobdc)(DMF)₂]@ polystyrene Composite and Its Carbon Dioxide Adsorption. *Microporous Mesoporous Mater.* **2016**, 232, 161–166.
- (59) Moreno, M. A.; Gálvez, O.; Maté, B.; Herrero, V. J.; Escribano, R. Formate Ion: Structure and Spectroscopic Properties. *J. Phys. Chem. A* **2011**, *115* (1), 70–75.
- (60) Choi, J. I.; Chun, H.; Lah, M. S. Zirconium-Formate Macrocycles and Supercage: Molecular Packing versus MOF-like Network for Water Vapor sorption. *J. Am. Chem. Soc.* **2018**, *140* (34), 10915–10920.
- (61) Lucier, B. E. G.; Zhang, Y.; Huang, Y. Complete Multinuclear Solid-State NMR of Metal-Organic Frameworks: The Case of α -Mg-Formate. Concepts Magn. Reson. Part A 2016, 45A (6), No. e21410.
- (62) Hanrahan, M. P.; Venkatesh, A.; Carnahan, S. L.; Calahan, J. L.; Lubach, J. W.; Munson, E. J.; Rossini, A. J. Enhancing the Resolution of ¹H and ¹³C Solid-State NMR Spectra by Reduction of Anisotropic Bulk Magnetic Susceptibility Broadening. *Phys. Chem. Chem. Phys.* **2017**, *19* (41), 28153–28162.
- (63) Cho, E.; Lee, T. S. Manipulation of Intramolecular Hydrogen Bonds in Single-Benzene Derivatives: Esterase Sensing, Fluorescence Patterning, and Inkless Writing. *Sens. Actuators B: Chem.* **2020**, 319, No. 128307.
- (64) Ren, X.; Wang, J.; Peng, Z.; Lu, L. Direct Monitoring of Trace Water in Li-Ion Batteries Using *Operando* Fluorescence Spectroscopy. *Chem. Sci.* **2018**, 9 (1), 231–237.
- (65) Della Pia, A.; Luo, D.; Blackwell, R.; Costantini, G.; Martsinovich, N. Molecular Self-Assembly of Substituted Terephthalic Acids at the Liquid/Solid Interface: Investigating the Effect of Solvent. *Faraday Discuss.* **2017**, 204, 191–213.
- (66) Denisov, G. S.; Golubev, N. S.; Schreiber, V. M.; Shajakhmedov, Sh. S.; Shurukhina, A. V. Excited State Intramolecular Proton Transfer and Dual Emission of the Cyclic Homo- and Heterodimers of 2-Hydroxy and 2,6-Dihydroxy Benzoic Acids. *J. Mol. Struct.* **1996**, *381* (1–3), 73–81.
- (67) Halder, A.; Bain, D. C.; Oktawiec, J.; Addicoat, M. A.; Tsangari, S.; Fuentes-Rivera, J. J.; Pitt, T. A.; Musser, A. J.; Milner, P. J. Enhancing Dynamic Spectral Diffusion in Metal—Organic Frameworks through Defect Engineering. J. Am. Chem. Soc. 2023, 145 (2), 1072—1082
- (68) Musser, A. J.; Rajendran, S. K.; Georgiou, K.; Gai, L.; Grant, R. T.; Shen, Z.; Cavazzini, M.; Ruseckas, A.; Turnbull, G. A.; Samuel, I. D. W.; Clark, J.; Lidzey, D. G. Intermolecular States in Organic Dye Dispersions: excimers vs. Aggregates. *J. Mater. Chem. C* **2017**, *5* (33), 8380–8389.
- (69) Yu, J.; Park, J.; Van Wyk, A.; Rumbles, G.; Deria, P. Excited-State Electronic Properties in Zr-Based Metal—Organic Frameworks as a Function of a Topological Network. *J. Am. Chem. Soc.* **2018**, *140* (33), 10488–10496.
- (70) Deria, P.; Yu, J.; Smith, T.; Balaraman, R. P. Ground-State versus Excited-State Interchromophoric Interaction: Topology Dependent Excimer Contribution in Metal—Organic Framework photophysics. *J. Am. Chem. Soc.* **2017**, *139* (16), 5973—5983.
- (71) Tang, B.; Liu, H.; Li, F.; Wang, Y.; Zhang, H. Single-Benzene Solid Emitters with Lasing Properties Based on Aggregation-Induced Emissions. *Chem. Commun.* **2016**, *52* (39), *6577*–6580.
- (72) Cheng, X.; Wang, K.; Huang, S.; Zhang, H.; Zhang, H.; Wang, Y. Organic Crystals with Near-Infrared Amplified Spontaneous Emissions Based on 2'-Hydroxychalcone Derivatives: Subtle Structure Modification but Great Property Change. *Angew. Chem., Int. Ed.* **2015**, 54 (29), 8369–8373.
- (73) Cheng, X.; Li, F.; Han, S.; Zhang, Y.; Jiao, C.; Wei, J.; Ye, K.; Wang, Y.; Zhang, H. Emission Behaviors of Unsymmetrical 1,3-Diaryl-β-Diketones: A Model Perfectly Disclosing the Effect of Molecular Conformation on Luminescence of Organic Solids. *Sci. Rep.* **2015**, *5* (1), 9140.

- (74) de Oliveira, A.; de Lima, G. F.; De Abreu, H. A. Structural and Electronic Properties of M-MOF-74 (M = Mg, Co or Mn). *Chem. Phys. Lett.* **2018**, *691*, 283–290.
- (75) Leith, G. A.; Martin, C. R.; Mayers, J. M.; Kittikhunnatham, P.; Larsen, R. W.; Shustova, N. B. Confinement-Guided photophysics in MOFs, COFs, and Cages. *Chem. Soc. Rev.* **2021**, *50* (7), 4382–4410.
- (76) Rice, A. M.; Martin, C. R.; Galitskiy, V. A.; Berseneva, A. A.; Leith, G. A.; Shustova, N. B. photophysics Modulation in Photoswitchable Metal—Organic Frameworks. *Chem. Rev.* **2020**, *120* (16), 8790—8813.
- (77) Dolgopolova, E. A.; Rice, A. M.; Martin, C. R.; Shustova, N. B. Photochemistry and photophysics of MOFs: Steps towards MOF-Based Sensing Enhancements. *Chem. Soc. Rev.* **2018**, 47 (13), 4710–4728.
- (78) Wang, Z.; Li, Z.; Ng, M.; Milner, P. J. Rapid Mechanochemical Synthesis of Metal—Organic Frameworks Using Exogenous Organic Base. *Dalton Trans.* **2020**, 49 (45), 16238–16244.
- (79) Chen, E. Y.; Mandel, R. M.; Milner, P. J. Evaluating Solvothermal and Mechanochemical Routes towards the Metal—Organic Framework Mg₂(*m*-dobdc). *CrystEngComm* **2022**, 24 (41), 7292–7297.